electronics

Article

Modular Battery Emulator for Development and Functional Testing of Battery Management Systems: Hardware Design and Characterization

Alessandro Verani , Roberto Di Rienzo *, Niccolò Nicodemo , Federico Baronti , Roberto Roncella and Roberto Saletti

Dipartimento di Ingegneria dell'Informazione, University of Pisa, Via Caruso 16, 56122 Pisa, Italy
* Correspondence: roberto.dirienzo@unipi.it

Abstract: Battery Management Systems are essential for safe and effective use of Lithium-Ion batteries. The increasing complexity of the control and estimation algorithms requires deeper functional testing and validation phases of BMSs. However, the use of real batteries in such phases leads to hazards and safety risks. Battery emulators and the Hardware-in-the-Loop approach can instead speed-up and increase the safety of the functional testing and algorithm validation phases. This work describes the design and the characterization of a low-cost modular multi-cell battery emulator which provides a complete emulation of cell voltage, temperature, and current. This platform can be used to carry out Hardware-in-the-Loop tests on custom and commercial Battery Management Systems. The paper describes the platform design constraints derived from the most diffused Battery Management System architectures, the main design and implementation choices, and the platform characterization results. The proposed emulation platform is compared with literature and commercial ones showing a very good trade-off between performance and cost. This characteristic makes it appealing for small-size laboratories that develop and test Battery Management Systems. The project has therefore been made available to the scientific community as a freely downloadable open hardware platform.

Keywords: battery management system; battery emulator; hardware in the loop; open hardware platform; BMS characterization

check for updates

Citation: Verani, A.; Di Rienzo, R.; Nicodemo, N.; Baronti, F.; Roncella, R.; Saletti, R. Modular Battery Emulator for Development and Functional Testing of Battery Management Systems: Hardware Design and Characterization. *Electronics* **2023**, *12*, 1232. https://doi.org/10.3390/electronics12051232

Academic Editors: Fortunato Pezzimenti, Antonio Di Bartolomeo, Davide Astolfi, Alessandro Ruvio and Gianpaolo Vitale

Received: 20 January 2023
Revised: 1 March 2023
Accepted: 2 March 2023
Published: 4 March 2023

1. Introduction

Lithium-Ion batteries are the most widespread energy storage technology thanks to their high power and energy densities, long cycle life, and low self-discharge rate [1]. Nevertheless, the working conditions of these batteries must be carefully monitored to ensure their safe usage and prevent degrading and destructive phenomena [2–4]. Such safety functions are accomplished by specific devices, the Battery Management Systems (BMSs) [5–7]. BMSs are usually based on a modular approach [8,9], and their functionalities are divided into different hierarchical levels [10,11]. The BMS reliability, both in terms of construction and noise immunity, is very important to guarantee the battery safety [12–14]. This is particularly true in safety-critical applications, such as the space and automotive ones [15,16]. For these reasons, the BMS hardware and software functions must be extensively tested [17,18].

Unfortunately, functional tests and control algorithm assessment are among the most complex and time-consuming phases of the Lithium-Ion BMS development. The Hardware-in-the-Loop (HiL) approach speeds up and simplifies those phases by replacing the battery with an emulator that mimics the battery behavior in a reproducible and controllable way [19–21]. The HiL platform provides the BMS inputs and acquires its responses comparing them with the expected values to check their correctness. Moreover, the HiL platform allows one to carry out BMS functional tests with voltage, current, and temperature values even outside the Lithium-Ion (Li-Ion) battery safe operating area to verify the BMS behavior and identify potentially harmful malfunctions [22].

HiL platforms can be classified according to their architecture in two main categories: communication HiL and power HiL [23]. In the communication HiL, an information flow is settled between the HiL platform and the BMS under test. The communication HiL platform simulates the battery behaviors and shares the cell voltage, current, and temperature to the BMS control system by injecting data in the communication bus of the BMS acquisition system. This architecture allows the accurate control of the simulated quantities and is therefore particularly useful in assessing safety and state estimation algorithms. On the other hand, it is highly architecture-specific and strictly depends on the BMS communication interface to its analog front-end. Moreover, it does not allow the complete assessment of the BMS functionalities, such as the verification of the balancing system. Instead, the power HiL approach replicates in a controlled and reproducible way the analog quantities monitored by the BMS under test. Therefore, power HiL platforms are less specific to the architecture of the BMS under test and enable the complete evaluation of the BMS functionalities. On the other hand, power HiL is usually expensive and requires the management of high power levels.

Several commercial and custom power HiL battery emulators have been developed in the last several years [24–35]. High complexity solutions using microcontrollers [26,32,33], DSPs [24], dual active bridge converters [36], and FPGAs [25] have been reported in the literature, together with low-cost solutions using simple analog circuits [28]. Usually, those emulators reproduce only the cell voltages of a variable number of series-connected cells that compose the "virtual battery", neglecting the emulation of the battery current and temperatures. This omission represents a major drawback in BMS functionalities assessment, since current and temperature measures are both essential to the safety function and to the State of Charge [37,38] and State of Health [39] estimation algorithms. These algorithms are fundamental in large battery packs such as those used in electric and hybrid vehicles. The battery control and state estimation algorithms play a key role in these applications to optimize the energy management strategies [40,41].

To the best of our knowledge, both commercial and custom power HiL battery emulators do not provide a complete all-in-one solution for emulation of voltages, current, and temperatures. The purpose of our project is to fill this gap by means of the development of a low-cost and open hardware/software platform. The platform is able to emulate the cell voltage and the output of current and temperature sensors of a battery composed of a variable number of series-connected cells. Small companies and laboratories could greatly benefit from such a simple and low-cost HiL platform, as it can be used to speed up the development and testing of new BMSs or third-party ones. For this purpose, the project sources are freely downloadable from [42].

Our project started in [43], where different circuit approaches to emulate the cell voltage were compared. The most promising architecture was also used to implement a single cell voltage emulator board that was experimentally characterized to highlight its pros and cons. The present work improves the cell voltage emulator submodule developed in [43] and illustrates the hardware design of the proposed all-in-one battery emulator including the new cell temperature and current emulation submodules. The design constraints of the platform are derived from the typical specifications of state-of-the-art BMSs. The hardware design is described and the realized circuit boards are extensively characterized and compared with literature and commercial solutions.

The main contributions of this work can be summarized as follows:

- Definition of the HiL platform structure based on modular approach to achieve the maximum platform flexibility and testing capabilities;
- Complete redesign of the previously released cell voltage emulator [43] addressing its major weakness, i.e., the maximum output current and the current measurement accuracy;
- Design of two additional submodules for the emulation of the temperature sensor outputs and the current sensor based on the Hall effect;

- Design of the rack based structure to arrange the voltage, temperature, and current submodules;
- Extensive experimental characterization of the platform submodules to investigate their advantages and disadvantages, and comparison of the obtained results with the literature and commercial solutions.

The remainder of this paper is organized as follows: Section 2 reports the main considerations about the BMS design used to define the emulator design constraints. The description of the emulator platform and the design of the submodules are described in detail in Section 3, while the characterization tests and the obtained results are discussed in Section 4. The comparison of the developed emulator with other literature and commercial solutions is shown in Section 5. Finally, some conclusions are drawn in Section 6.

2. Design Constraints of the Battery Emulator Platform

Functional test and algorithm assessment of the BMS requires the validation of several possible scenarios and the complete and accurate emulation of all the battery behaviors. For this reason, an emulation platform is a very complex and usually expensive system [34]. For example, checking the safety control functions requires that the emulator should be able to sink and source very high currents and generate cell voltages and temperature variations consistent with a certain battery model. Luckily, strategies can be adopted to keep the system complexity low, still allowing the validation of the BMS functions. For example, the battery emulator can generate the analog output of the current and temperature sensors to deceive the BMS. This solution allows one to stimulate and validate the BMS functions but does not allow the validation of the current and temperature sensors instead. However, such step can easily be performed separately by characterizing the sensors used, independently from the BMS.

The definition of the design constraints is essential to obtain a versatile battery emulator while keeping its cost and complexity as low as possible. The constraints are directly derived from the BMS characteristics and are summarized in the following subsections.

2.1. Cell Voltage Emulator Constraints

The cell voltage emulator constraints were discussed in detail in [43]. In particular, the emulated voltage range should include all the possible values of the Li-Ion technologies, resulting in an interval from 1.5 to 4.5 V. The maximum output current should be high enough to check all the battery functionalities such as the balancing algorithm. The BMS balancing circuit can be based on a large number of approaches and architectures [44,45]. However, the balancing current usually goes from some tens of milliamperes to a few amperes in passive and active balancing systems [31,46], respectively. Therefore, a reasonable constraint for the maximum sink/source output current is around 1 A. The setting voltage resolution and the maximum update frequency constraints are related to the measurement circuit of the BMS under test. The cell voltage acquisition is usually accomplished by the BMS using an Analog to Digital Converter (ADC) with up to 16 bits of resolution and a reference value of 5 V. The voltage reading frequency is usually lower than 10 Hz, but it can reach over 100 Hz in some critical battery applications. Finally, the output of the cell voltage emulator must be isolated to allow the series connection of multiple emulated cells to build up the battery.

2.2. Current Emulator Design Constraints

Hall-effect based current sensors are one of the most common solutions for current sensing in battery applications [47,48]. They intrinsically ensure galvanic isolation between power and sensing paths and no voltage drop. Their output is a voltage proportional to the flowing current in most cases. Table 1 reports the main characteristics of some of the most common commercial Hall-based current sensors. These characteristics are used as design constraints for the current sensor emulator submodule, to achieve good compatibility with the reported sensors.

Table 1. Specifications of commercial current sensor based on the Hall effect.

Manufacturer	Device Series	Output Range	Load Specification
CR Magnetics Inc.	CR 5200	$-5 \div 5$ V $-10 \div 10$ V	$R_L > 2\,\mathrm{k\Omega}$
Honeywell Sensing and Productivity Solutions	CSCA	$-12 \div 12$ V	$R_L > 10\,\mathrm{k\Omega}$
LEM USA Inc.	LES, LESR, LKSR LPSR, LXS, LXSR HAS, HX	$0 \div 5$ V $-12 \div 12$ V	$R_L > 10\,\mathrm{k\Omega}$ $C_L < 100\,\mathrm{nF}$ $R_L > 10\,\mathrm{k\Omega}$
Tamura	L01Z, L06P, S05 L03S	$0.5 \div 4.5$ V $-12 \div 12$ V	$R_L > 10\,\mathrm{k\Omega}$

It can be seen that the possible output voltage value can be either unipolar with $0 \div 5$ V range or bipolar with $-12 \div 12$ V range. The output of the current sensor is generally acquired using a 14 or 16 bit ADC. The sampling period of the current value is generally between 100 ms and 1 s, but it can reach 1 ms for specific applications, e.g., in the presence of current pulses.

2.3. Temperature Emulator Constraints

Temperature sensing can be accomplished using three main types of sensors: integrated thermal sensors, thermocouples, and thermistors. The most common choice in BMSs is thermistors, i.e., resistors, the resistance of which strongly depends on the temperature, since they are easy to read, cheap, and do not require additional communications [47,49]. The thermistor values are typically read by the BMS using an ADC with 10 or 12 bit and a sampling rate lower than 10 Hz. The ADC reads the voltage V_{ADC} on the thermistor $R(T)$ by applying a reference voltage V_{REF} to a voltage divider obtained with the thermistor and a series-connected reference resistor R_{REF} [49]:

$$V_{\mathrm{ADC}} = V_{\mathrm{REF}} \frac{R(T)}{R_{\mathrm{REF}} + R(T)} \quad \text{with} \quad R(T) = R(T_0)\, e^{\beta\left(\frac{1}{T} - \frac{1}{T_0}\right)} \tag{1}$$

$R(T_0)$ is the resistance of the thermistor at a reference temperature T_0, usually 25 °C, and β is a parameter of the thermistor. Therefore, the thermistor's value can be emulated by an analog voltage generator. Since the resistor values are in the order of tens of kiloohms, and the emulator output must ensure an output current of at least 1 mA for each emulated sensor. An update frequency of 10 Hz is adequate for the emulation of the temperature sensors.

3. Battery Emulator Platform Design

The constraints described in the previous section are summarized in Table 2 and are used to design the battery emulator. The hardware of the proposed battery emulator is composed of a variable number of series-connected standard modules. This architecture allows us to adapt the size of the platform to the BMS under test.

Table 2. Design constraints of the three submodules.

Feature	Cell Voltage Emulator	Current Emulator	Temperature Emulator
Output range	$0.5 \div 4.5$ V	$-12 \div 12$ V	$0 \div 5$ V
Output resolution	$\geq$16 bit	$\geq$14 bit	$\geq$10 bit
Output update frequency	$\geq$100 Hz	$\geq$1 kHz	$\geq$10 Hz
Maximum continuous sink/source current	$1 \div 2$ A	$\geq$10 mA	$\geq$1 mA per channel
Maximum capacitive load	No requirements	$\geq$100 nF	No requirements

The proposed battery emulator operates as shown in Figure 1. A proper number of standard modules are series-connected to emulate the number of cells required by the BMS under test. The battery emulator is controlled using a graphical user interface on a PC, which checks the platform working status and configures its submodules to emulate a given battery behavior. In addition, the BMS interface can be run on the same host PC to perform BMS configuration and to check BMS functionalities. The data read by the BMS and those imposed by the emulator are compared to check possible inconsistencies and malfunctions. Such validation can be performed by the operator or by an additional software program that automatically performs the data check and the BMS characterization process.

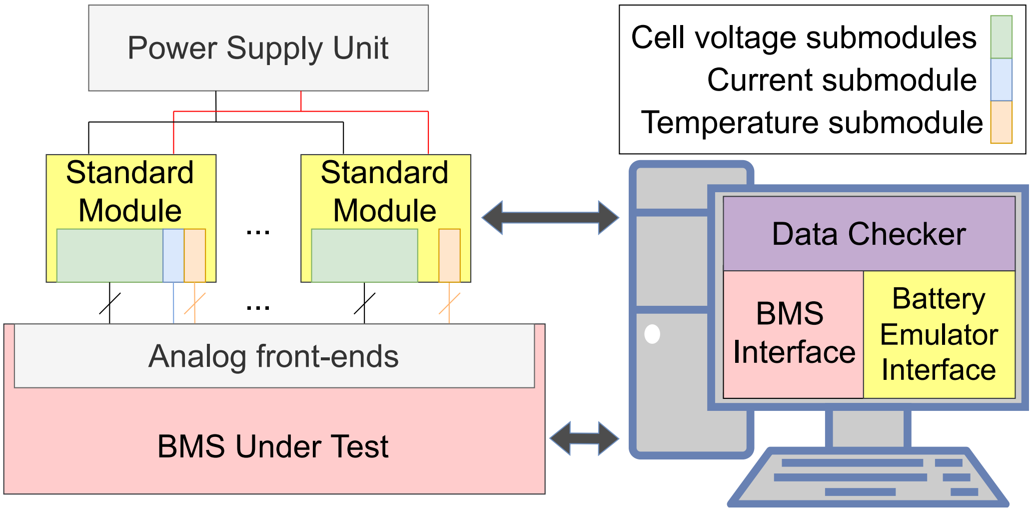

Figure 1. Block scheme of the testing environment of the proposed battery emulator.

Each standard module emulates up to eight series-connected cells and is based on a rack structure composed of an interconnection board which can be equipped with up to eight cell voltage submodules, one temperature submodule with eight channels, one current submodule, and a control board. The interconnection board is provided with an edge card connector for each submodule and external connectors for the submodule outputs, the power supply, and the external communications. Moreover, vertical supports prevent the insertion of a submodule in the wrong connector and provide the possibility to mount two 80 mm cooling fans. The rack structure allows the battery emulator upgrade by adding or replacing submodules without changing the entire platform. The general block diagram of the standard module and its 3D rendering are shown in Figure 2.

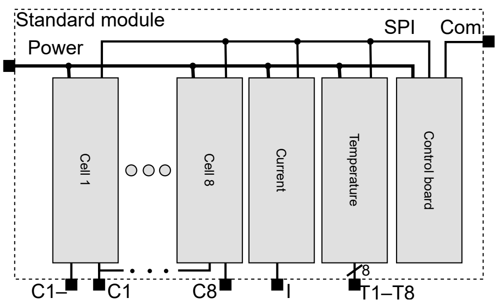

(**a**)

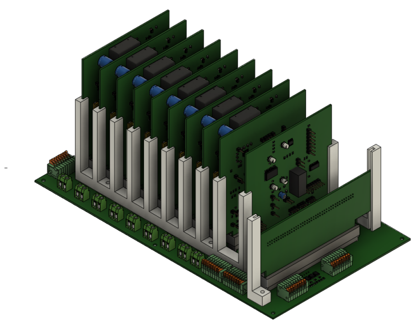

(**b**)

Figure 2. Standard module of the developed platform: Block diagram (**a**) and 3D rendering (**b**).

The control board is connected to the other submodules via a Serial Peripheral Interface (SPI) bus, and all the submodules are powered by a 48 V power bus. This high voltage value was chosen to reduce the maximum bus current, when all the cell submodules provide the maximum output current. It is also important to note that the outputs of the cell voltage emulator submodules are series-connected; therefore, the input power bus and the communication bus of each submodule must be isolated. The hardware description of the control board is omitted in this paper because it is strictly related to the software parts of the platform that is under development. For this reason, this board will be described in a future work.

Submodules Design

The architectures of the submodules that emulate the voltage, the current, and the temperature are very similar to each other and are shown in Figure 3. The core of the architecture consists of a Digital to Analog Converter (DAC) and an Analog to Digital Converter (ADC). The DAC is used to set the board output voltage (eight independent outputs are present in the temperature sensor emulator board) that is conditioned according to the quantity to be emulated by an analog circuit different in the three board types. The ADC, instead, measures the board output quantities. Both of these converters are controlled by the control board via the isolated SPI bus. The submodules have also been equipped with an isolated DC/DC converter that generates the supply voltages needed. If the board requires multi voltage levels, one or more linear DC/DC converters are connected to the isolated DC/DC output. The minimum isolation voltage guaranteed by the isolation devices is 600 V. It limits the maximum emulated battery voltage and then the number of series-connected standard modules. The maximum emulated battery voltage is equal to the product of the total number of series-connected cells by the maximum cell voltage (5 V). The components of each board type were chosen to guarantee the design constraints reported in Section 2 minimizing the system cost and complexity.

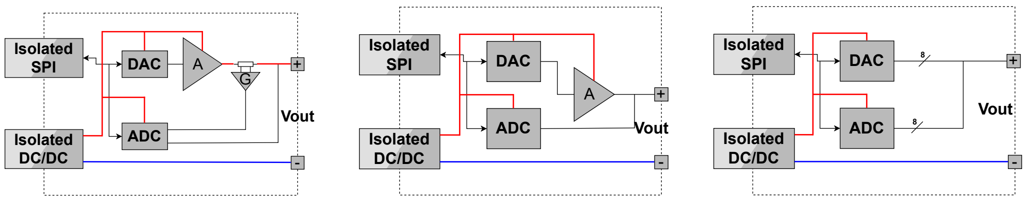

(**a**) (**b**) (**c**)

Figure 3. Architecture of cell voltage emulator (**a**); current sensor emulator (**b**); temperature sensor emulator (**c**).

The cell voltage submodule is based on a 16 bit DAC, the DAC8501 from Texas Instruments. It generates the input voltage of the operational amplifier OPA569 from Texas Instruments, which is connected as a non-inverting amplifier with gain A equal to 2. The operational amplifier provides a rail-to-rail output with a configurable maximum output current up to 2 A. This operational amplifier allows us to improve the performance of the cell voltage emulator submodule presented in [43] by increasing the maximum output current.

The accuracy of the current measurement system is one of the major weaknesses of the previous cell voltage emulator version [43]. For this reason, the current measurement architecture has been significantly changed and relies on a 5 mΩ shunt resistor connected in series to the operational amplifier output, instead of the Hall-based current sensor of the first version. The feedback path of the operational amplifier is taken after the shunt resistor, to allow the automatic compensation of the voltage drop on the shunt itself. The voltage drop across the shunt resistor is then amplified by the Current-Sense amplifier INA186, from Texas instruments, with a differential gain of 50. A 16 bit Sigma-Delta ADC, the Microchip Technology MCP3464, is used to acquire both the emulator output voltage and the output of INA186. Finally, the board can be equipped with an additional OPA569, parallel-connected to the first one, to increase the maximum output current of the board.

However, the submodule design allows the user to replace the shunt current measuring system with a Hall-based current sensor, the TMCS1101 from Texas Instruments.

The output level of the current sensor submodule is controlled using the same DAC of the cell submodule and a rail-to-rail operational amplifier with low input offset, the OPA196 by Texas Instruments. The operational amplifier adjusts the output range from -12 to $12\,\mathrm{V}$ with a theoretical resolution of $366\,\mu\mathrm{V}$. A resistor R_{iso} can be series-connected to the output of the operational amplifier to increase its stability in the case of a high capacitive load, reducing the output bandwidth. The output voltage is sensed by a 14 bit SAR ADC, the Texas Instruments ADS8675, which has a software-configurable input voltage range from -12.288 to $12.288\,\mathrm{V}$. Finally, the board output can also be optimized to cover the 0 to $5\,\mathrm{V}$ output range by means of an appropriate configuration of the operational amplifier resistor network.

An 8-channel 12 bit DAC, the Texas Instruments DAC128S085, is used for the temperature submodule board, to directly generate the eight independent outputs. A 12 bit 8-channel SAR ADC, the Texas Instruments TLV2548, is used to acquire the board outputs. The choice of ADC and DAC with eight channels optimizes the trade-off between complexity and cost of the battery emulator design, allowing for emulating eight independent temperature sensor outputs.

The boards were designed using the free software suite for electronic design KiCad EDA [50]. The project source files can freely be downloaded from [42].

4. Characterization of the Standard Module

A standard module consisting of four cell voltage, one current, and one temperature submodules was assembled and characterized. Figure 4 shows the characterization experimental setup. The TTi QPX1200SP, on the left-hand side of the figure, provides the power supply to the standard module. Then, a sourcemeter Keithley 2460 is connected to the output of one submodule. It imposes a controlled output current and measures the output values that are used as reference to verify the accuracy of the submodule. The sourcemeter is also connected to a custom LabVIEW interface which configures the instrument and logs the acquired data. The sourcemeter is connected by the operator to the particular submodule that is going to be characterized. A Python script running on a PC was developed to implement the control board functionalities, i.e., setting and reading the output values of the submodule under test. The communication between the PC and the standard module is accomplished with an USB to SPI converter, the Microchip Technology MCP2210. All the tests were performed at room temperature. The current value is considered positive if sourced by the platform.

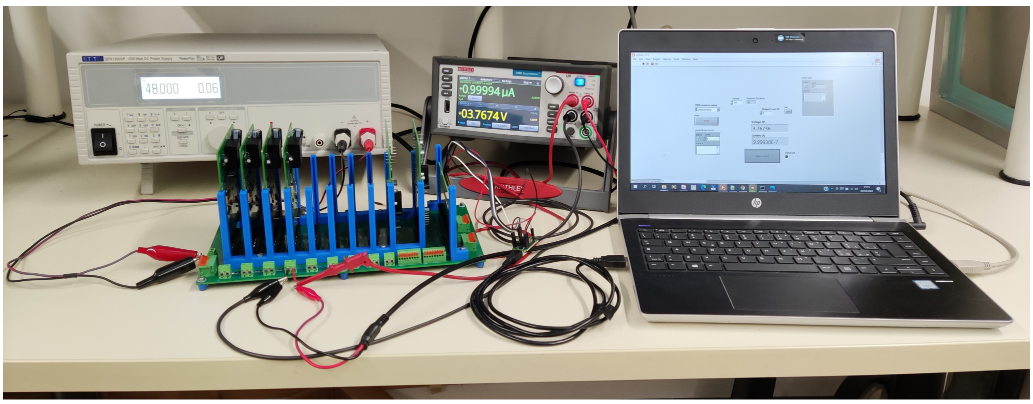

Figure 4. Experimental setup used for the characterization of the battery emulator module.

4.1. Cell Voltage Submodule

The cell voltage submodule was validated using test routines very similar to the ones presented in [43]. A sweep of the DAC output code from 0 to the maximum value with an output current equal to zero is used to characterize the cell voltage submodule output stage.

Ten samples for each DAC code are acquired from the onboard ADC and from the Keithley sourcemeter. They are compared one to the other to assess both the set and read accuracies. Each theoretical set value is compared with the mean value of the relative 10 samples acquired by the sourcemeter to obtain the set accuracy of the emulator. Instead, the read accuracy is obtained by subtracting from the mean value read by the ADC the reference value measured by the sourcemeter. Figure 5a,b report the set and the read errors, respectively.

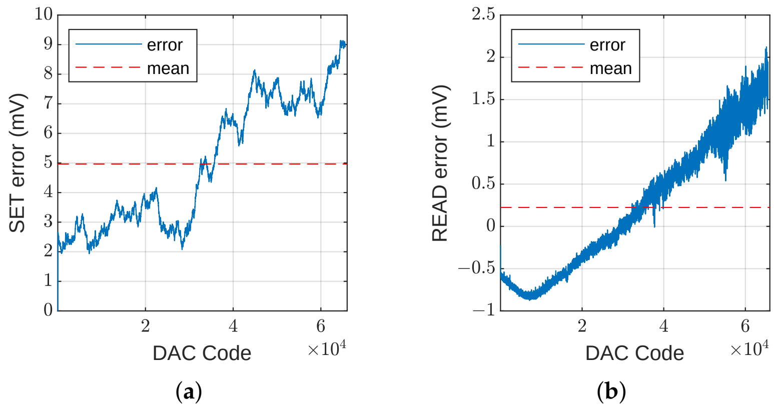

Figure 5. Characterization of the set (**a**) and read (**b**) error with no output current.

We note that the voltage set error varies from about 2 to 9 mV with an average value of 4.96 mV and a standard deviation of 2.15 mV. The maximum error is less than 0.2% of the full-scale value, showing a good overall accuracy of the cell voltage submodule. The read error instead varies from about −1 to 2 mV, with a standard deviation of only 0.78 mV. This result demonstrates a very good accuracy of the onboard measurement system, enabling the use of the ADC reading as feedback to partially correct the set error. In fact, the set error can further be reduced by correcting via software the output voltage value. Tests with non-zero output current were performed to characterize the current measurement system and the output voltage with different load levels. A thermal analysis was preliminarily performed to establish the maximum current levels that the board can sink and source. The power dissipated by the operational amplifier (P_{diss}) can be expressed as [43]:

$$\begin{cases} P_{\text{diss}} = (V_{\text{cc}} - V_{\text{out}}) I_{\text{out}} & \text{if} \quad I_{\text{out}} > 0 \\ P_{\text{diss}} = -V_{\text{out}} I_{\text{out}} & \text{if} \quad I_{\text{out}} < 0 \end{cases} \tag{2}$$

where V_{cc} is the power supply voltage (5 V), and V_{out} and I_{out} are the output voltage and current, respectively. Since the desired output range varies from 0.5 to 4.5 V, the worst-case scenarios for the power dissipated by the operational amplifier are with V_{out} equal to 0.5 V when it sources current and V_{out} equal to 4.5 V when it acts as sink. The maximum current level was evaluated by means of a Flir i50 infrared camera, with which the current is found that brings the operational amplifier from room temperature to the temperature of 125 °C, a value close to the absolute maximum rating of the device. The current value results in being ±750 mA. Figure 6 shows the image acquired by the infrared camera after 15 min when sourcing 750 mA with a V_{out} of 0.5 V. This result shows 50% improvement in the maximum output current with respect to the previous version of the cell voltage submodule presented in [43]. Figure 6 also shows that the heat produced by the operational amplifier causes a thermal gradient over the board surface. This gradient also affects the behavior of the shunt resistor, which is visible on the left side of Figure 6. A shunt resistor with low thermal electromotive force coefficient must be used to avoid voltage drifts due to thermoelectric effects [51]. Since the proposed standard module provides room to place two cooling fans, the same test condition of V_{out} equal to 0.5 V was applied with the fans switched on, achieving a further improved maximum I_{out} of 1.25 A. This current value is sufficient to validate BMS either with passive balancing or active balancing techniques, even for high-capacity battery packs.

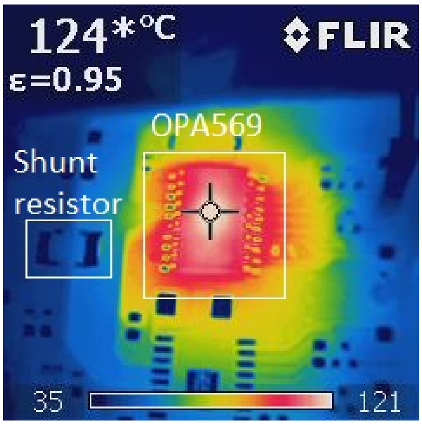

Figure 6. Thermal image of the OPA569 measured with a Flir50 infrared camera. It shows a maximum steady state temperature of 124 °C. The measurement was taken after 15 min of a constant power (3.37 W) stress test.

The board was also characterized at different current levels. The submodule output voltage is varied from 0.5 to 4.5 V with steps of 0.5 V while the current value is changed from −750 mA to 750 mA with steps of 250 mA for each voltage step. Each current step has a duration of 300 s to characterize both the voltage output behavior with respect to the current value and the possible thermal effect due to the heating of the operational amplifier. The output current is held at 0 for 300 s after each step to let the circuit cool down. The first 10 samples of the acquired quantities are averaged. Then, the average is compared to the reference to determine the effects of the output current on the output voltage errors. The set and read errors are reported in the upper diagrams of Figure 7a,b, respectively.

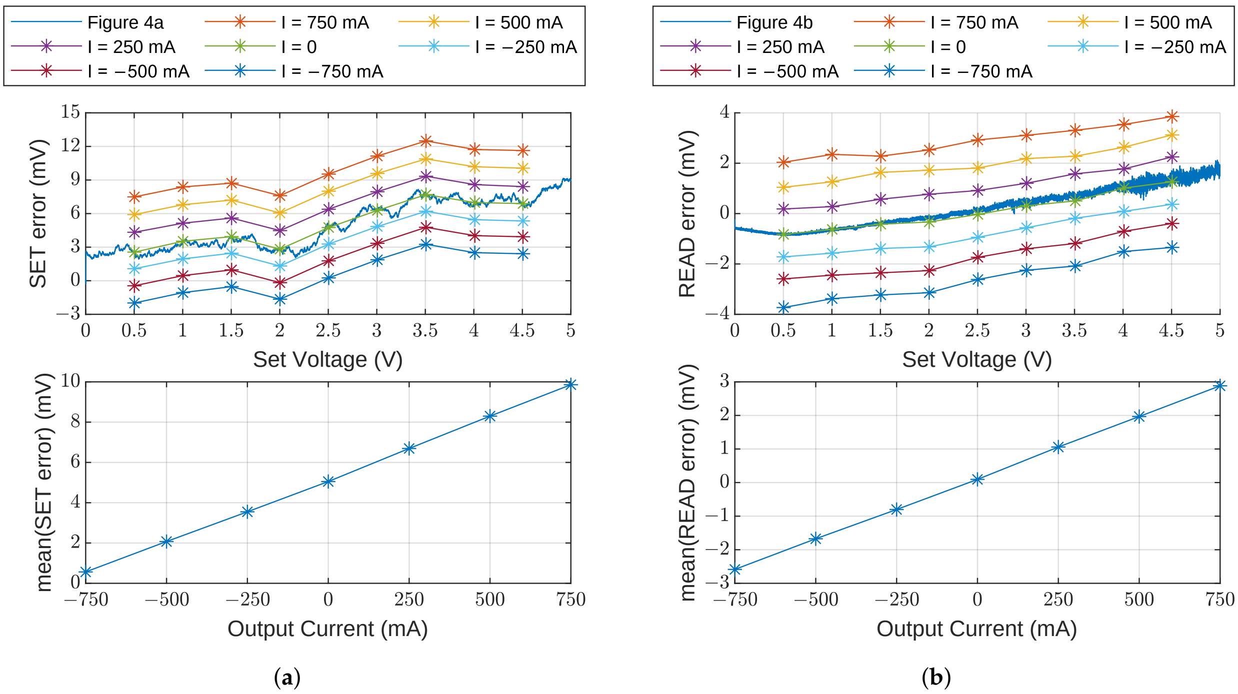

Figure 7. Set voltage error (**a**) and read voltage error (**b**) with different cell current values. Errors versus the set value (**top**). Mean set and read errors as a function of the output current (**bottom**).

The continuous diagrams in the top figures show the set and the read errors measured in the previous tests of Figure 5. We see that the errors with zero output current are almost perfectly superimposed, even if they are obtained with two very different tests, showing the repeatability of the results. Moreover, the diagrams with non-zero output current are almost parallel one to the other. Thus, the emulator output can be modeled with a voltage generator and a series resistor. The resistance value can be estimated starting from the data shown in the bottom diagrams of Figure 7a,b, which report the mean error values for each output current level. The curves are an almost perfect straight line with a slope of 6.19 mΩ and 3.6 mΩ for the set and read error, respectively. These results can also be used to easily correct via software the effect of the current, if needed.

Then, the average of the first 10 reference voltage samples and the last 10 ones of each current pulse are compared to identify any potential thermal dependency of the output voltage value. The set error difference between the two mean values taken at the beginning and end of the test is always less than 0.62 mV, showing a very low dependence of the set error on the operational amplifier temperature. The current measurement error I_{err} is calculated by applying the same procedure, as the difference between the mean value of the first 10 samples of the ADC data and the reference one. The upper part of Figure 8 shows I_{err} as a function of the set voltage for the considered output current values. The bottom part of Figure 8 instead reports the mean value of the current measurement error for each imposed current value.

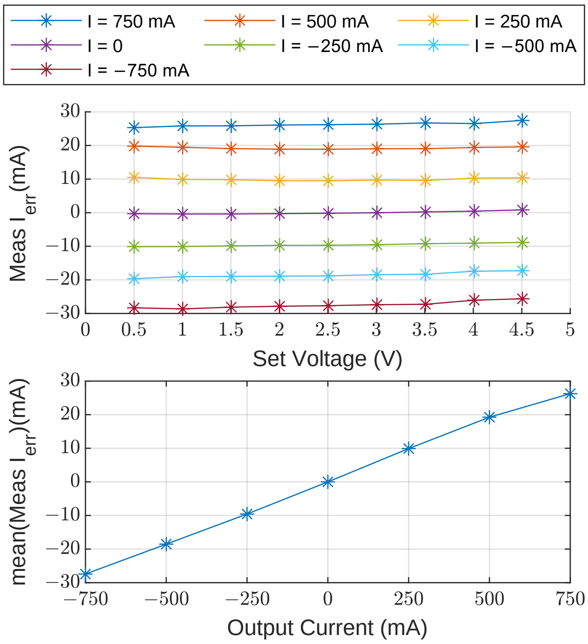

Figure 8. Characterization of the current measurement system error with different cell current values. Error as a function of the cell voltage set for different output current (**top**); mean current measurement error as a function of the output current (**bottom**).

The results show a good accuracy of the onboard current measurement system, which presents a negligible offset and a gain error of about 4%. In fact, the curve in the bottom part of Figure 8 can linearly be interpolated with the function $a + b * I_{out}$, with a equal to -0.02 mA and b equal to 0.037. This gain error is compatible with the overall accuracy of the submodule current measurement system. However, it could easily be corrected with a calibration procedure. These results represent a significant improvement of the onboard current measurement system compared to the previous version of the cell voltage emulator submodule presented in [43]. In fact, that version presented a nonlinear behavior of the error and a mean value significantly different from zero.

Finally, the maximum update frequency of the output was evaluated by means of a Tektronix MS056 oscilloscope, by performing a step change of the output value from the minimum to the maximum with current values of -750, 0, and 750 mA. The response time consists of two main contributions: the time needed to configure the DAC and the settling time of the operational amplifier. The DAC configuration time is composed of two parts: the communication time, which strictly depends on the chosen SPI speed and on the number of bits required for the DAC configuration, and the time needed by the DAC to update its output value. The chosen DAC requires three bytes for its configuration. Thus, the configuration time is about 24 µs using a SPI communication speed of 1 Mbit/s. This time can further be reduced increasing the communication speed up to 20 Mbit/s if needed. The sum of the "DAC data to output" value and the operational amplifier settling time was measured using the oscilloscope. The maximum value obtained is 27 µs. The sum of the two contributions enables an update time of about 51 µs and therefore a maximum update frequency of about 20 kHz, in compliance with the 100 Hz constraint reported in Table 2.

4.2. Current Sensor Emulator Submodule

A very similar characterization procedure was carried out on the current sensor emulator submodule. First, a complete sweep of the DAC codes with a load current of 0, ±5 mA, and ±10 mA was performed. The set and read errors obtained are reported in Figure 9. The error curves obtained with different output currents are very similar one to the other, except for an offset error. The set error for the no load current test has a mean value of 48.14 mV and a standard deviation of 8.94 mV in the worst case. However, the maximum relative error is less than 0.32% of the output full scale that complies with the required emulator accuracy. The read error shows a mean value of −8.83 mV and a standard deviation of 0.99 mV in the worst case. The high accuracy of the onboard ADC can be used to improve the output set value using the measured quantity as feedback.

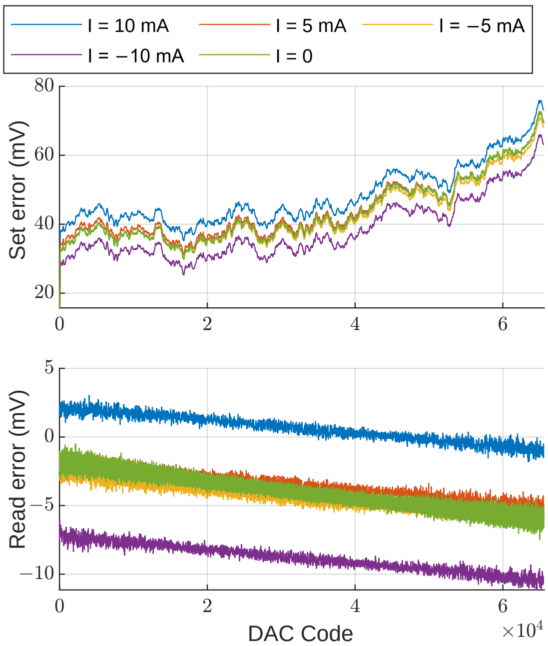

Figure 9. Characterization of set error (**top**) and read error (**bottom**) of current emulator board with different output current values.

The maximum steady state temperature reached by the operational amplifier is about 65 °C in the worst-case scenario with a sink current of 10 mA. Moreover, the maximum update frequency can be estimated with the same procedure used for the cell voltage submodule. In this case, the worst time from the DAC configuration to the stable output is 108 µs, achieved with a communication speed of 1 Mbit/s. It corresponds to a maximum update frequency of about 9.2 kHz that meets the specification. Finally, a ceramic capacitor of 100 nF was connected between the output terminals to test the capability to drive capacitive loads. A 12 V to 0 step and a −12 V to 0 steps were performed, and the output voltage was measured. This choice allows the maximum possible ringing and maintains the output in the middle of its dynamic range. Test results suggest that a value of 120 Ω for the output series resistance R_{iso} provides a good trade-off between stability and set time.

4.3. Temperature Sensor Emulator Submodule

The temperature submodule was also tested using a similar procedure. The complete sweep of the DAC codes with no load was applied to all the output channels, and the set and read errors were measured. For the sake of clarity, Figure 10a reports the errors obtained for the first channel only, as the other channels show very similar behaviors. The set error mean varies from −1.22 to −5.11 mV among the eight channels, while the standard deviation varies from 1.01 to 2.33 mV. Instead, the read error mean varies from 6.58 to 10.43 mV, with a standard deviation that varies from 4.53 to 5.02 mV.

These output voltage errors can be converted in temperature errors. Let us consider the typical application of thermistors in BMS described in Section 2.3 and summarized with Equation (1). The voltage set error is converted in a set temperature error using V_{REF} equal to 5 V, R_{REF} and $R(T_0)$ equal to 10 kΩ, T_0 equal to 25 °C, and β equal to 3450. The calculated set temperature error is shown in Figure 10b. The gray areas in the figure represent temperature values outside −40 ÷ 125 °C, which is the operating range of the thermistor chosen as an example.

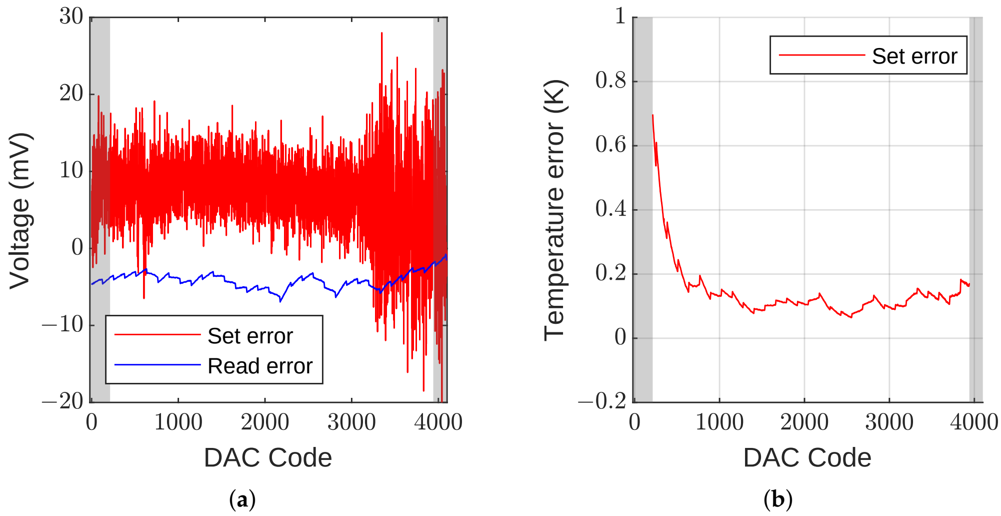

Figure 10. Characterization of set error and read error of the first channel of temperature emulator board with no output current. Set error and read error as a function of the set value (**a**); voltage set error converted in a temperature error (**b**).

Figure 10b shows that the set temperature error is always less than 0.8 °C, and is less than 0.2 °C for the major part of the settable temperature range. The obtained results prove that our solution represents a good trade-off between cost and performance, allowing the utilization of this board for the emulation of the temperature sensors of the battery.

Since the output voltage of the board is directly driven by the DAC, the maximum settling time can be taken from the datasheet that indicates less than 8.5 µs. Therefore, the minimum update frequency constraint of 10 Hz can also be reached at low communication speed. The maximum continuous current for each channel is 6.5 mA as reported in the device datasheet.

5. Discussion and Future Developments

The experimental results meet the constraints presented in Table 2 for all the three developed submodules. The major weaknesses of the platform stand in the set accuracy of the current sensor submodule and in the read accuracy of the temperature sensor one, which show a significant absolute error. However, the set and read errors obtained for all the submodules comply with the requirements and the accuracy of the typical analog front-end usually implemented in state-of-the-art BMSs. The same consideration could also be drawn for the update frequency and current level. The proposed battery emulator is here compared both with literature and commercial solutions. To the best of our knowledge, an all-in-one platform including temperature and current sensors has not been presented in the literature yet. The authors propose a battery cell voltage emulator platform based on an hierarchical approach in [24]. Each cell voltage is emulated by means of a microcontroller unit with internal DAC and a power amplifier stage. Instead, the authors propose a cell architecture similar to ours in [26], but they use a microcontroller unit for each cell voltage emulation board. Finally, we include in the comparison the previous version of our cell voltage emulator shown in [43]. Table 3 summarizes the comparison results concerning the cell voltage emulation. The temperature and current submodules are not included in this comparison because these functionalities are not provided by the other works.

Table 3. Feature comparison of our work with literature solutions.

Work	**[24]**	**[26]**	**Our Previous Work [43]**	**Our Work**
Cell Architecture	OPAMP + µC with internal 12 bit DAC/ADC	OPAMP + µC + external 16 bit DAC/ADC	OPAMP + external 16 bit DAC/ADC	OPAMP + external 16 bit DAC/ADC
Voltage resolution	1.2 mV	92 µV	76 µV	76 µV
Voltage accuracy	±1.2 mV [1]	±270 µV [2]	±2.17 mV [3]	±2 mV [3]
Maximum current	3 ÷ 5 A	3 A	0.5 A	1.25 A
Current accuracy	2 mA [1]	±462 µA [2]	±19.6 mA [3]	±25 mA [3]
Set time	5 µs	1.26 µs	340 µs	51 µs
Cost	low	medium	very low	very low

[1] Theoretical data; [2] Spice simulation results; [3] With offset correction.

It is worth noting that the results of our solutions are obtained with experiments, while the others are theoretical or extracted from simulations. The weakest point of our solution is the current measurement accuracy, which is slightly greater than the others. However, this inaccuracy is due to gain errors and can easily be corrected by means of software calibration. Table 3 also highlights that our new version of the cell voltage emulator submodule provides better characteristics of the previous one at the same cost. In particular, the major upgrades are the extension of the current range from ±0.5 A to ±1.25 A and a significant reduction of the set time.

To fairly compare our solution with commercial ones, the economic aspect must also be considered. A coarse estimated cost of the three submodules and the backplane is: 60$ for each cell, 50$ for the current sensor emulator, 50$ for the current sensor emulator, and 40$ for the backplane, including the PCB printing and mounting services. Therefore, a complete standard module cost is around 620$.

Three commercial battery emulators (Keithley Series 2281S, NXP BATT-6EMULATOR, and NGI N83624) are also compared with our battery emulation platform. Keithley Series 2281S consists of a single channel DC power supply that is able to emulate the cell voltage using a predefined or custom battery model. The NXP BATT-6EMULATOR emulates up to six cells in series, using a slide potentiometer to configure the cell voltage output values. Furthermore, it provides an additional channel to emulate a shunt resistor voltage drop in a range of ±150 mV. NGI N83624 provides 24 isolated channels in the range 0 to 5 V to emulate the cell voltages and an application software to control the channels behavior. Table 4 reports the feature comparison between our solution and the above-mentioned ones. For the sake of clarity, the costs reported in the table are the sell prices for the commercial devices and the prototype production cost for our solution.

Table 4. Feature comparison of our work with commercial solutions.

Feature	Keithley Series 2281S [52]	NXP BATT-6Emulator [53]	NGI N83624 [54]	Our Work
Software configurable	YES	NO	YES	YES
# of cells per module	1	6	24	8
Maximum countinous sourced current per channel	6 A	115 mA	1 A, 3 A, or 5 A configuration available	1.25 A with fan (0.75 A no fan)
Maximum countinous sink current per channel	1 A	NO	NO	1.25 A with fan (0.75 A no fan)
Cell voltage resolution	1 mV	Slider	0.1 mV	76 µV
Cell voltage set accuracy	±0.2% + 2 mV	Slider	1 mV	∼9 mV
Current and Temperature CHs	Not Available	1 CH for shunt emulation ±150 mV	some of the 24 CHs (0 ÷ 5 V) can be used	8 temperature CHs (0 ÷ 5 V) 1 CH for current (−12 ÷ 12 V)
Price/Cost	≥3 k$	∼500$	some k$	620$

Table 4 shows that our platform provides a very good trade-off between performance and cost. In fact, its cost is comparable to the NXP BATT-6Emulator, but it offers a software configurable solution, two additional cell voltage channels, bidirectional current, a maximum output current ten times larger, and eight additional channels for temperature sensor emulation. Moreover, our platform has a performance comparable to that of the NGI N83624 and Keithley Series 2281S solutions, but its cost is much lower. The development of a control board and a custom graphical interface to set and read the output values of the platform is under development and will be presented in future works. The final goal will be to provide the community with a user-friendly interface to directly control the platform output quantities or to apply different battery models, e.g. the simple resistance or the two RC-branch models [55], that reproduce the behavior of a real battery. The developed HiL platform is published under the Open Hardware License and adds a new piece to the low-cost open hardware system for Lithium-Ion testing proposed in [56,57].

6. Conclusions

The design and the experimental characterization of a low-cost battery emulator for BMS testing and verification using the Hardware-in-the-Loop approach are presented in this work. The battery emulator is designed using a modular approach where each module emulates up to eight cell voltages, eight temperature sensors, and a Hall-based current sensor. The module is based on a rack structure where each emulation function is provided by a specific submodule. One submodule emulates the cell voltage in a range from 0.5 to 4.5 V with a maximum continuous current of ±750 mA. The second submodule emulates eight temperature sensor outputs with eight independent voltage signals from 0 to 5 V. The last one emulates the output voltage of a Hall-based current sensor with a range of ±12 V.

The measured set errors of the cell voltage, temperature, and current submodules are less than 0.2%, 0.32%, and 0.6% of the full scale values, respectively. The obtained results prove that the developed platform is a good hardware solution suitable for both BMS functional tests and the development of battery control algorithms. Furthermore, a comparison with commercial battery emulators is presented and highlights the very good trade-off between cost and performance of the proposed solution with respect to the commercial ones.

Author Contributions: Conceptualization, A.V., N.N. and R.D.R.; methodology, R.D.R.; software, A.V.; validation, A.V. and N.N.; formal analysis, A.V., N.N. and R.D.R.; investigation, A.V. and N.N.; resources, R.D.R.; data curation, A.V. and N.N.; writing—original draft preparation, A.V., N.N. and R.D.R.; writing—review and editing, F.B., R.R. and R.S.; visualization, A.V.; supervision, F.B., R.R. and R.S.; project administration, R.S.; funding acquisition, R.R. All authors have read and agreed to the published version of the manuscript.

Funding: This research was partially funded by the PNRR Sustainable Mobility Center (Centro Nazionale per la Mobilità Sostenibile—CNMS)—CN00000023—CUP I53C22000720001, and supported by the Italian Ministry of Education and Research (MIUR) in the framework of the FoReLab project (Departments of Excellence).

Data Availability Statement: The project archive of the described battery emulator is made available to the community as an open hardware resource at https://github.com/batterylabunipi/Modular_Battery_Emulator, accessed on 10 January 2023.

Conflicts of Interest: The authors declare no conflict of interest.

References

1. Dutta, A.; Mitra, S.; Basak, M.; Banerjee, T. A comprehensive review on batteries and supercapacitors: Development and challenges since their inception. *Energy Storage* **2023**, *5*, e339. [CrossRef]
2. Feng, C.; Yang, X. Explosion mechanism and prevention of lithium-ion batteries. In Proceedings of the 2019 IEEE Sustainable Power and Energy Conference (iSPEC), Beijing, China, 21–23 November 2019; pp. 969–974. [CrossRef]
3. Thingvad, M.; Calearo, L.; Thingvad, A.; Viskinde, R.; Marinelli, M. Characterization of NMC Lithium-ion Battery Degradation for Improved Online State Estimation. In Proceedings of the 2020 55th International Universities Power Engineering Conference (UPEC), Turin, Italy, 1–4 September 2020; pp. 1–6. [CrossRef]
4. Chen, Z.; Huang, P.; Pang, Q.; Gu, P.; Duan, B.; Zhang, C. Thermal runaway analysis and model of nickel-rich lithium-ion batteries in different overcharging states. In Proceedings of the 2022 6th CAA International Conference on Vehicular Control and Intelligence (CVCI), Nanjing, China, 28–30 October 2022; pp. 1–6. [CrossRef]
5. Gabbar, H.A.; Othman, A.M.; Abdussami, M.R. Review of Battery Management Systems (BMS) Development and Industrial Standards. *Technologies* **2021**, *9*, 28. [CrossRef]
6. Wei, Z.; Zhao, J.; He, H.; Ding, G.; Cui, H.; Liu, L. Future smart battery and management: Advanced sensing from external to embedded multi-dimensional measurement. *J. Power Sources* **2021**, *489*, 229462. [CrossRef]
7. Xing, Y.; Ma, E.W.; Tsui, K.L.; Pecht, M. Battery Management Systems in Electric and Hybrid Vehicles. *Energies* **2011**, *4*, 1840–1857. [CrossRef]
8. Canilang, H.M.O.; Caliwag, A.C.; Lim, W. Design of Modular BMS and Real-Time Practical Implementation for Electric Motorcycle Application. *IEEE Trans. Circuits Syst. II Express Briefs* **2022**, *69*, 519–523. [CrossRef]
9. Zhang, R.; Wu, J.; Wang, R.; Yan, R.; Zhu, Y.; He, X. A Novel Battery Management System Architecture Based on an Isolated Power/Data Multiplexing Transmission Bus. *IEEE Trans. Ind. Electron.* **2019**, *66*, 5979–5991. [CrossRef]
10. Waldhoer, S.; Bockrath, S.; Wenger, M.; Schwarz, R.; Lorentz, V.R.H. foxBMS-free and open BMS platform focused on functional safety and AI. In Proceedings of the PCIM Europe Digital Days 2020; International Exhibition and Conference for Power Electronics, Intelligent Motion, Renewable Energy and Energy Management, Nuremburg, Germany, 7–8 July 2020; pp. 1–6. [CrossRef]
11. Di Rienzo, R.; Baronti, F.; Vellucci, F.; Cignini, F.; Ortenzi, F.; Pede, G.; Roncella, R.; Saletti, R. Experimental analysis of an electric minibus with small battery and fast charge policy. In Proceedings of the 2016 International Conference on Electrical Systems for Aircraft, Railway, Ship Propulsion and Road Vehicles & International Transportation Electrification Conference (ESARS-ITEC), Toulouse, France, 2–4 November 2016; pp. 1–6. [CrossRef]
12. See, K.W.; Wang, G.; Zhang, Y.; Wang, Y.; Meng, L.; Gu, X.; Zhang, N.; Lim, K.C.; Zhao, L.; Xie, B. Critical review and functional safety of a battery management system for large-scale lithium-ion battery pack technologies. *Int. J. Coal Sci. Technol.* **2022**, *9*, 36. [CrossRef]
13. Aiello, O.; Crovetti, P. Characterization of the Susceptibility to EMI of a BMS IC for Electric Vehicles by Direct Power and Bulk Current Injection. *IEEE Lett. Electromagn. Compat. Pract. Appl.* **2021**, *3*, 101–107. [CrossRef]
14. Weijie, Z.; Youjie, S.; Bo, L. Functional safety analysis and design of BMS for lithium-ion battery energy storage system. *Energy Storage Sci. Technol.* **2020**, *9*, 271. [CrossRef]
15. Verani, A.; Fieramosca, G.; Colicelli, A.; Di Rienzo, R.; Saletti, R.; Roncella, R.; Schwarz, R.; Lorentz, V.; Baronti, F. FPGA Accelerator for Battery Management Systems in Safety-Critical Applications. In Proceedings of the 2020 2nd IEEE International Conference on Industrial Electronics for Sustainable Energy Systems (IESES), Cagliari, Italy, 1–3 September 2020; Volume 1, pp. 261–266. [CrossRef]
16. Anand, M.D.; Reshmi, S.; Mercy, T.; Jacob, T.; Devi, S.A. Lithium-ion cells for space applications: Aspects of durability. *Adv. Space Res.* **2023**. [CrossRef]
17. Aiello, O. Electromagnetic Susceptibility of Battery Management Systems' ICs for Electric Vehicles: Experimental Study. *Electronics* **2020**, *9*, 510. [CrossRef]
18. Doridant, A.; Abouda, K.; Givelin, P.; Thibaud, B. Battery Management System Demonstrator Board design using EMC System simulation. In Proceedings of the 2019 International Symposium on Electromagnetic Compatibility—EMC EUROPE, Barcelona, Spain, 2–6 September 2019; pp. 427–432. [CrossRef]
19. Wu, H. Hardware-in-loop verification of battery management system. In Proceedings of the 2011 4th International Conference on Power Electronics Systems and Applications, Hong Kong, China, 8–10 June 2011; pp. 1–3. [CrossRef]

20. Preetha, V.; Vavilapalli, K.; Jeevan, N.K.; Abilash, P. Model-based Hardware-in the-Loop Testing of Battery Management System; SAE Technical Papers. In Proceedings of the 10th SAE India International Mobility Conference (SIIMC), Bangalore, India, 12–14 October 2022. [CrossRef]
21. Ponchant, M.; Li, A.; Beckers, C.; Paroha, M. Battery Management System Evaluation within a Complete Electric Vehicle Model with Software-in-the-Loop and Hardware-in-the-Loop Approaches. In Proceedings of the 2021 23rd European Conference on Power Electronics and Applications, EPE'21 ECCE Europe, Ghent, Belgium, 6–10 September 2021. [CrossRef]
22. Sun, B.; Zhao, X.; He, X.; Ruan, H.; Zhu, Z.; Zhou, X. Virtual Battery Pack-Based Battery Management System Testing Framework. *Energies* **2023**, *16*, 680. [CrossRef]
23. Barreras, J.V.; Fleischer, C.; Christensen, A.E.; Swierczynski, M.; Schaltz, E.; Andreasen, S.J.; Sauer, D.U. An Advanced HIL Simulation Battery Model for Battery Management System Testing. *IEEE Trans. Ind. Appl.* **2016**, *52*, 5086–5099. [CrossRef]
24. Collet, A.; Crébier, J.C.; Chureau, A. Multi-cell battery emulator for advanced battery management system benchmarking. In Proceedings of the 2011 IEEE International Symposium on Industrial Electronics, Gdansk, Poland, 27–30 June 2011; pp. 1093–1099. [CrossRef]
25. van Sterkenburg, S.; Fleuren, T.; Veenhuizen, B.; Groenewegen, J. Design and test of a battery pack simulator. In Proceedings of the 2013 World Electric Vehicle Symposium and Exhibition (EVS27), Barcelona, Spain, 17–20 November 2013; pp. 1–12. [CrossRef]
26. Buccolini, L.; Orcioni, S.; Longhi, S.; Conti, M. Cell Battery Emulator for Hardware-in-the-Loop BMS Test. In Proceedings of the 2018 IEEE International Conference on Environment and Electrical Engineering and 2018 IEEE Industrial and Commercial Power Systems Europe (EEEIC/I&CPS Europe), Palermo, Italy, 12–15 June 2018; pp. 1–5. [CrossRef]
27. Bischof, S.; Kuecuek, C.; Blank, T.; Weber, M. A Battery Cell Emulator for Hardware in the Loop Tests of Reconfigurable Lithium-Ion and Post-Lithium Batteries. In Proceedings of the PCIM Europe 2018; International Exhibition and Conference for Power Electronics, Intelligent Motion, Renewable Energy and Energy Management, Nuremberg, Germany, 5–7 June 2018; pp. 1–7. [CrossRef]
28. Di Rienzo, R.; Roncella, R.; Morello, R.; Baronti, F.; Saletti, R. Low-cost modular battery emulator for battery management system testing. In Proceedings of the 2018 IEEE International Conference on Industrial Electronics for Sustainable Energy Systems (IESES), Hamilton, New Zealand, 31 January–2 February 2018; pp. 44–49. [CrossRef]
29. Mishra, S.; Tamballa, S.; Pallantala, M.; Raju, S.; Mohan, N. Cascaded Dual-Active Bridge Cell Based Partial Power Converter for Battery Emulation. In Proceedings of the 2019 20th Workshop on Control and Modeling for Power Electronics (COMPEL), Toronto, ON, Canada, 17–20 June 2019; pp. 1–7. [CrossRef]
30. Bui, T.M.N.; Niri, M.F.; Worwood, D.; Dinh, T.Q.; Marco, J. An Advanced Hardware-in-the-Loop Battery Simulation Platform for the Experimental Testing of Battery Management System. In Proceedings of the 2019 23rd International Conference on Mechatronics Technology (ICMT), Salerno, Italy, 23–26 October 2019; pp. 1–6. [CrossRef]
31. Tschritter, C.D.; Wetz, D.A.; Turner, G.K.; Heinzel, J.M. Battery Management System (BMS) Test Stand Utilizing a Hardware-in-the-Loop (HIL) Emulated Battery. In Proceedings of the 2021 IEEE Electric Ship Technologies Symposium, ESTS, Arlington, VA, USA, 3–6 August 2021. [CrossRef]
32. Högerl, T.; Buberger, J.; Schwitzgebel, F.; Obkricher, L.; Estaller, J.; Hohenegger, M.; Kersten, A.; Kuder, M.; Eckerle, R.; Weyh, T. Battery Emulation for Battery Modular Multilevel Management (BM3) Converters and Reconfigurable Batteries with Series, Parallel and Bypass Function. In Proceedings of the 2021 IEEE International Conference on Environment and Electrical Engineering and 2021 IEEE Industrial and Commercial Power Systems Europe (EEEIC / I&CPS Europe), Bari, Italy, 7–10 September 2021. [CrossRef]
33. Santoni, F.; Angelis, A.D.; Moschitta, A.; Carbone, P. Digital Impedance Emulator for Battery Measurement System Calibration. *Sensors* **2021**, *21*, 7377. [CrossRef]
34. Li, R.; Ji, Y.; Fu, Y.; Hu, B.; Hu, H. Design and implementation of a parametric battery emulator based on a power converter. *IET Electr. Power Appl.* **2022**, *16*, 1300–1316. [CrossRef]
35. Khalid, A.; Stevenson, A.; Sarwat, A.I. Performance Analysis of Commercial Passive Balancing Battery Management System Operation Using a Hardware-in-the-Loop Testbed. *Energies* **2021**, *14*, 8037. [CrossRef]
36. Dash, S.; Chandorkar, M. Battery Emulation Using Dual-Active Bridge Converter. In Proceedings of the 2019 National Power Electronics Conference, NPEC, Tiruchirappalli, India, 13–15 December 2019. [CrossRef]
37. Rahimi-Eichi, H.; Ojha, U.; Baronti, F.; Chow, M.Y. Battery management system: An overview of its application in the smart grid and electric vehicles. *IEEE Ind. Electron. Mag.* **2013**, *7*, 4–16. [CrossRef]
38. Morello, R.; Di Rienzo, R.; Roncella, R.; Saletti, R.; Schwarz, R.; Lorentz, V.; Hoedemaekers, E.; Rosca, B.; Baronti, F. Advances in Li-Ion Battery Management for Electric Vehicles. In Proceedings of the IECON 2018—44th Annual Conference of the IEEE Industrial Electronics Society, Washington, DC, USA, 21–23 October 2018; pp. 4949–4955. [CrossRef]
39. Li, Q.; Li, D.; Zhao, K.; Wang, L.; Wang, K. State of health estimation of lithium-ion battery based on improved ant lion optimization and support vector regression. *J. Energy Storage* **2022**, *50*, 104215. [CrossRef]
40. Li, J.; Wu, X.; Xu, M.; Liu, Y. A real-time optimization energy management of range extended electric vehicles for battery lifetime and energy consumption. *J. Power Sources* **2021**, *498*, 229939. [CrossRef]
41. Zhang, F.; Xiao, L.; Coskun, S.; Pang, H.; Xie, S.; Liu, K.; Cui, Y. Comparative study of energy management in parallel hybrid electric vehicles considering battery ageing. *Energy* **2022**, *264*, 123219. [CrossRef]

42. Modular Battery Emulator. Available online: https://github.com/batterylabunipi/Modular_Battery_Emulator (accessed on 21 February 2023). [CrossRef]
43. Rienzo, R.D.; Verani, A.; Baronti, F.; Roncella, R.; Saletti, R. Modular Battery Emulator for Development and Functional Testing of Battery Management Systems: The Cell Emulator. *Electronics* **2022**, *11*, 1215. [CrossRef]
44. Hua, Y.; Zhou, S.; Cui, H.; Liu, X.; Zhang, C.; Xu, X.; Ling, H.; Yang, S. A comprehensive review on inconsistency and equalization technology of lithium-ion battery for electric vehicles. *Int. J. Energy Res.* **2020**, *44*, 11059–11087. [CrossRef]
45. Qu, F.; Luo, Q.; Liang, H.; Mou, D.; Sun, P.; Du, X. Systematic Overview of Active Battery Equalization Structures: Mathematical Modeling and Performance Evaluation. *IEEE Trans. Energy Convers.* **2022**, *37*, 1685–1703. [CrossRef]
46. Rienzo, R.D.; Zeni, M.; Baronti, F.; Roncella, R.; Saletti, R. Passive balancing algorithm for charge equalization of series connected battery cells. In Proceedings of the 2020 2nd IEEE International Conference on Industrial Electronics for Sustainable Energy Systems, IESES, Cagliari, Italy, 1–3 September 2020; pp. 73–79. [CrossRef]
47. Lelie, M.; Braun, T.; Knips, M.; Nordmann, H.; Ringbeck, F.; Zappen, H.; Sauer, D.U. Battery Management System Hardware Concepts: An Overview. *Appl. Sci.* **2018**, *8*, 534. [CrossRef]
48. Vincent, T.A.; Gulsoy, B.; Sansom, J.E.H.; Marco, J. A Smart Cell Monitoring System Based on Power Line Communication—Optimization of Instrumentation and Acquisition for Smart Battery Management. *IEEE Access* **2021**, *9*, 161773–161793. [CrossRef]
49. Pham, N.N.; Leuchter, J.; Pham, K.L.; Dong, Q.H. Battery Management System for Unmanned Electric Vehicles with CAN BUS and Internet of Things. *Vehicles* **2022**, *4*, 639–662. [CrossRef]
50. KiCad EDA—Schematic Capture PCB Design Software. Available online: https://www.kicad.org/ (accessed on 21 February 2023). [CrossRef]
51. Verani, A.; Di Rienzo, R.; Baronti, F.; Roncella, R.; Saletti, R. Analysis of Thermal-Induced Shunt Current Sensor Errors in a Low-Cost Battery Management System. In *International Conference on Applications in Electronics Pervading Industry, Environment and Society*; Saponara, S., De Gloria, A., Eds.; Springer International Publishing: Cham, Switzerland, 2022; pp. 107–113. [CrossRef]
52. Test and Measurement Equipment | Tektronix. Available online: https://www.tek.com/en (accessed on 21 February 2023). [CrossRef]
53. NXP® Semiconductors Official Site | Home. Available online: https://www.nxp.com/ (accessed on 21 February 2023). [CrossRef]
54. Next, Generation Instrumental (Shanghai) T&C Tech. Co., Ltd. Available online: https://en.ngitech.cn/ (accessed on 21 February 2023). [CrossRef]
55. Morello, R.; Rienzo, R.D.; Roncella, R.; Saletti, R.; Baronti, F. Hardware-in-the-loop platform for assessing battery state estimators in electric vehicles. *IEEE Access* **2018**, *6*, 68210–68220. [CrossRef]
56. Carloni, A.; Baronti, F.; Rienzo, R.D.; Roncella, R.; Saletti, R. Open and Flexible Li-ion Battery Tester Based on Python Language and Raspberry Pi. *Electronics* **2018**, *7*, 454. [CrossRef]
57. Carloni, A.; Baronti, F.; Rienzo, R.D.; Roncella, R.; Saletti, R. An Open-Hardware and Low-Cost Maintenance Tool for Light-Electric-Vehicle Batteries. *Energies* **2021**, *14*, 4962. [CrossRef]